A Comparison among Observations and Earthquake Simulator Results for the allcal2 California Fault Model

by Terry E. Tullis, Keith Richards-Dinger, Michael Barall, James H. Dieterich, Edward H. Field, Eric M. Heien, Louise H. Kellogg, Fred F. Pollitz, John B. Rundle, Michael K. Sachs, Donald L. Turcotte, Steven N. Ward, and M. Burak Yikilmaz

Online Material: Supplemental figures of space-time and frequency-magnitude relations, scaling plots, mean and covariance plots of interevent times, probability distribution functions of recurrence intervals, and earthquake density plots.

INTRODUCTION

In order to understand earthquake hazards we would ideally have a statistical description of earthquakes for tens of thousands of years. Unfortunately the ~100-year instrumental, several 100-year historical, and few 1000-year paleoseismological records are woefully inadequate to provide a statistically significant record. Physics-based earthquake simulators can generate arbitrarily long histories of earthquakes; thus they can provide a statistically meaningful history of simulated earthquakes. The question is, how realistic are these simulated histories? This purpose of this paper is to begin to answer that question. We compare the results between different simulators and with information that is known from the limited instrumental, historic, and paleoseismological data.

As expected, the results from all the simulators show that the observational record is too short to properly represent the system behavior; therefore, although tests of the simulators against the limited observations are necessary, they are not a sufficient test of the simulators' realism. The simulators appear to pass this necessary test. In addition, the physics-based simulators show similar behavior even though there are large differences in the methodology. This suggests that they represent realistic behavior. Different assumptions concerning the constitutive properties of the faults do result in enhanced capabilities of some simulators. However, it appears that the similar behavior of the different simulators may result from the fault-system geometry, slip rates, and assumed strength drops, along with the shared physics of stress transfer.

This paper describes the results of running four earthquake simulators that are described elsewhere in this issue of *Seismological Research Letters*. The simulators ALLCAL (Ward, 2012), VIRTCAL (Sachs *et al.*, 2012), RSQSim (Richards-Dinger and Dieterich, 2012), and ViscoSim (Pollitz, 2012) were run on our most recent all-California fault model, allcal2. With the exception of ViscoSim, which ran for 10,000 years, all the simulators ran for 30,000 years. Presentations containing content similar to this paper can be found at http://scec.usc.edu/research/eqsims/.

FAULT MODEL

allcal2 is the fault model used for this work (Fig. 1). A detailed description of this model can be found at http://scec.usc.edu/research/eqsims/documentation.html, and a description of the formats used can be found in Barall (2012). The model is almost identical to the UCERF2 deformation model, which essentially used the same faults and slip rates. This model is discretized at a 3-km resolution and involves ~15, 000 square elements. The model is driven by backslip loading and assignment of fault strength drops for each fault section, as was described by Tullis *et al.* (2012).

RESULTS AND RELATED DISCUSSION

The fundamental result of each earthquake simulator is a catalog of simulated earthquakes. A graphical summary of earthquakes for this catalog is shown in Figure 2 for two of the simulators, ALLCAL and VIRTCAL. Ⓔ These figures and those for the other two simulators can be seen in Figures S1–S4 of the electronic supplement to this article, where they can be enlarged for more detailed viewing. Figure 2 illustrates that these two simulators show somewhat different numbers of earthquakes as a function of magnitude,

 doi: 10.1785/0220120094

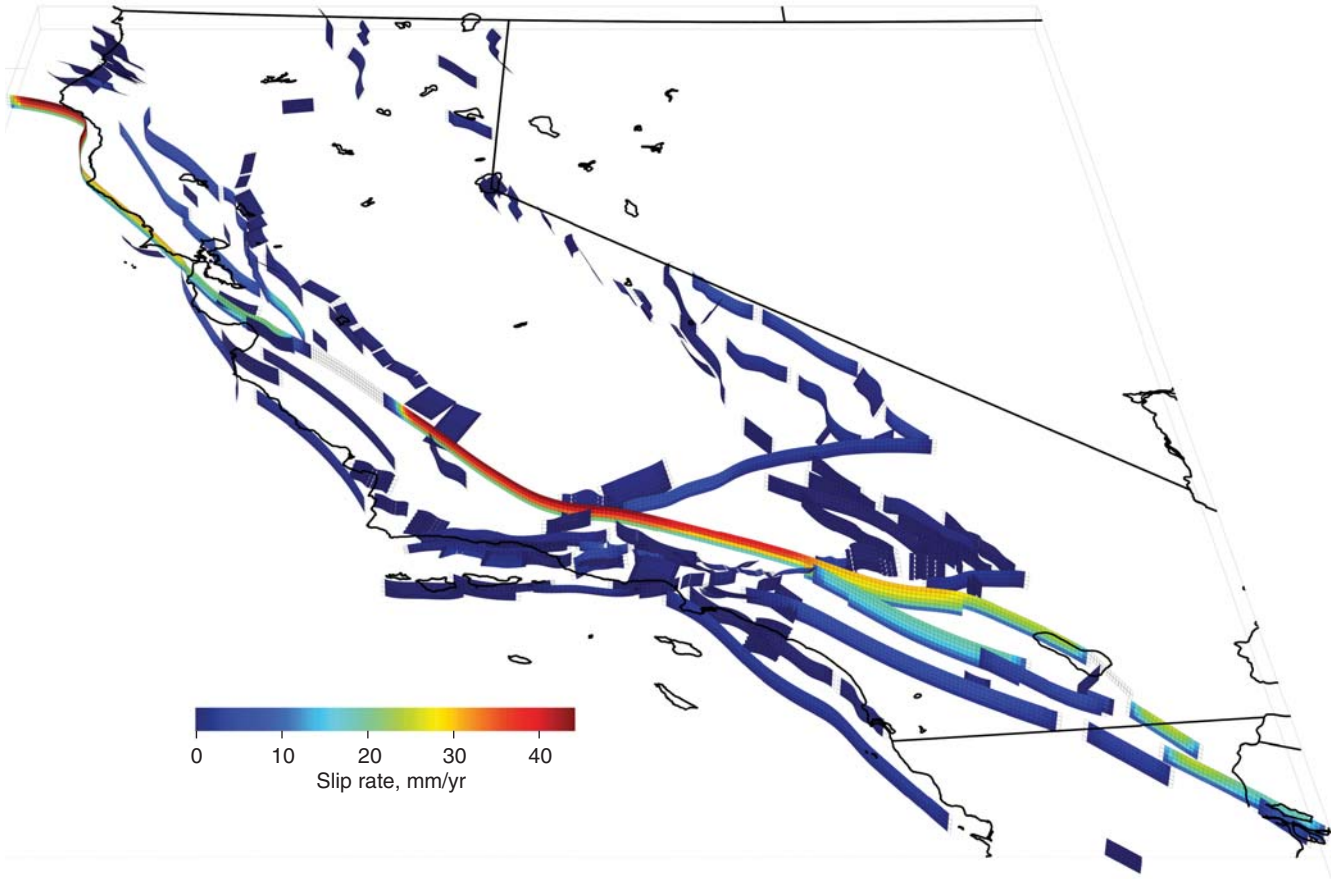

▲ **Figure 1.** Our allcal2 model, having ~15,000 elements, each an ~3-km square, extending to ~12 km depth. This is essentially the UCERF2 deformation model, including the illustrated average slip rate, which we impose by backslip (Tullis *et al.*, 2012).

with ALLCAL having more small events. This results from the choice made in VIRTCAL to set the rupture-weakening parameter (Tullis *et al.*, 2012) to a value which encourages smaller events to grow larger.

FREQUENCY-MAGNITUDE PLOTS

One of the more meaningful comparisons that can be made between the different simulators and the observations is shown in the frequency magnitude plot of Figure 3. The observational data come from figure 15 of the UCERF2 report (Field *et al.*, 2008) and represent about 100 years of instrumental data. As can be seen from the plot, nearly all the simulations lie between the 95% confidence intervals for the data, with ALLCAL and RSQSim lying closer to the mean of the data, and ViscoSim and VIRTCAL lying on either side. ViscoSim has smaller and fewer larger events, and VIRTCAL has fewer smaller events. The behavior of ViscoSim is explained by its not having a parameter that encourages rupture weakening; VIRTCAL behavior is explained by its setting a parameter so as to encourage rupture propagation. In this regard, it is interesting and somewhat surprising that ALLCAL and RSQSim behave similarly, yet ALLCAL has no rupture-weakening parameter and RSQSim has one (Tullis *et al.*, 2012). In fact, further examination reveals that RSQSim is closer to the observations between **M** 6 and **M** 7, whereas ALLCAL shows relatively more **M** 7 events, the opposite of what would be expected because ALLCAL lacks a rupture-weakening parameter. Our calculated magnitudes are in fact moment magnitudes, but we will refer to them as **M** rather than as M_w.

Note that below about **M** 6.5, VIRTCAL does not match the observations represented by the red curve in Figure 2. This was an intentional choice because many of the observed smaller earthquakes do not occur on the modeled faults, but rather on smaller known or unknown faults. This unmodeled background seismicity is envisioned as adding to the modeled seismicity, thereby producing the observed total seismicity. This decision is implemented by using a rupture-propagation parameter that encourages earthquakes to grow larger, and consequently fewer smaller earthquakes occur on the modeled faults.

Ⓔ Additional frequency-magnitude plots can be found in the electronic supplement. These include plots that show the variation among 15 random examples of 100-year periods of simulations (Fig. S5) and plots for specific faults, the north (Fig. S6) and south (Fig. S7) San Andreas fault and the San Jacinto (Fig. S8) fault. Ⓔ The plots of Figure S5 show that the trends noted above for each simulator hold true for all fifteen 100-year samples. However, only RSQSim

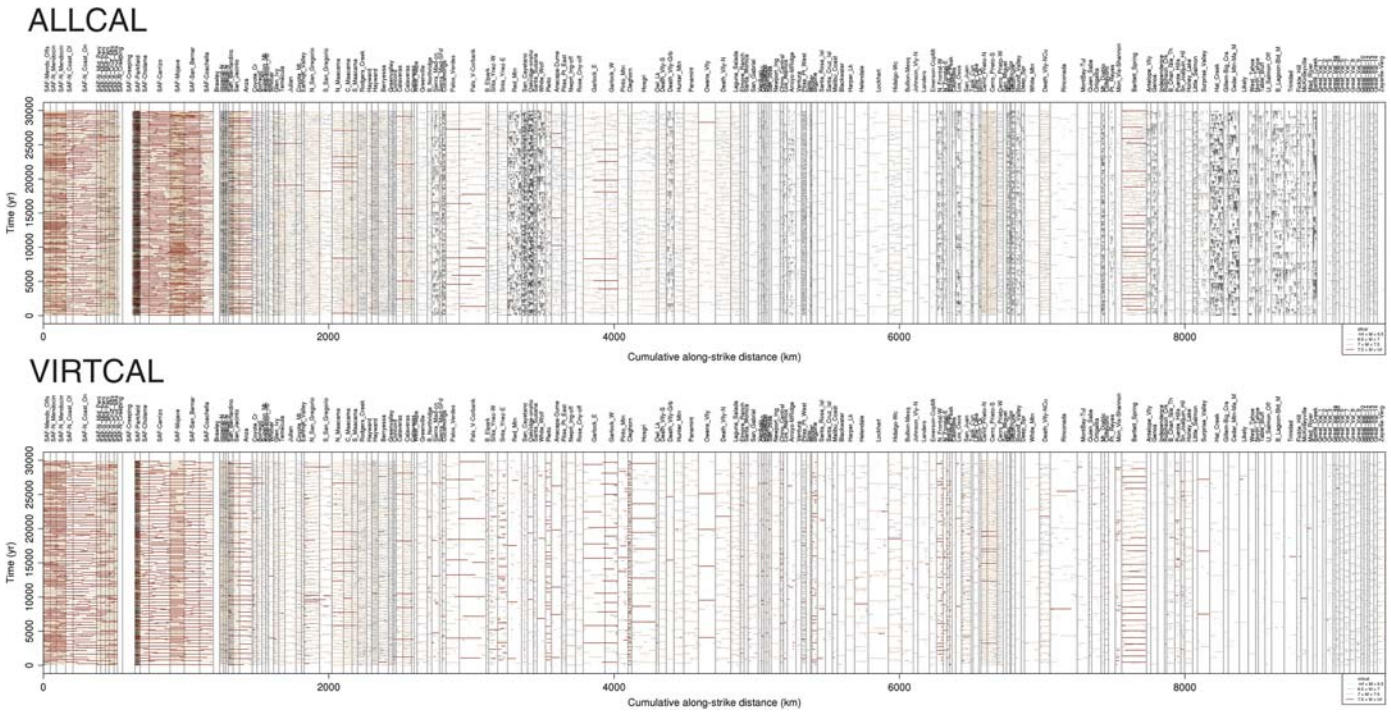

▲ **Figure 2.** Space-time plots for two simulators showing timing and sizes of earthquakes for all modeled fault sections. Ⓔ Electronic versions of these graphical catalogs of our simulated histories for all four simulators are Figures S1–S4 of the electronic supplement and can be enlarged to see more detail.

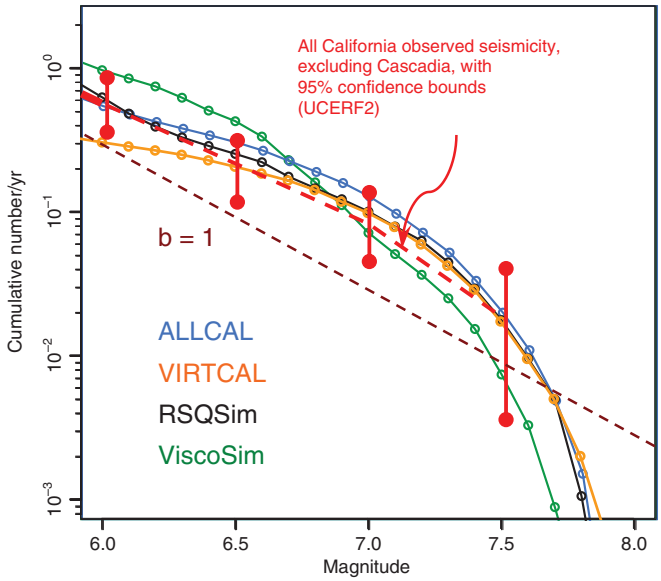

▲ **Figure 3.** The frequency-magnitude plot for four earthquake simulators compared with observations shown as a broken red line (fig. 15 of Field *et al.*, 2008). ALLCAL and RSQSim are quite similar to each other and to observations. This is less true for VIRTCAL and ViscoSim due to different assumptions made about weakening during rupture, which affects rupture propagation.

and VIRTCAL show several examples below and several above the 100-year observations of the UCERF2 report; this is only for VIRTCAL above **M** 6.5. The single-fault frequency-magnitude plots show that the number of events of **M** 7 and smaller is more reduced than at **M** 7.5 when compared to the entire data set. Thus, these plots show that the events on these faults are in some sense more characteristic than is the distribution when all the faults in the system are included.

MOMENT AND EVENT RATES

Plots of 100-year moving averages of moment and **M** 6+ and **M** 7+ event rates for all the simulators are shown in Figure 4, together with the UCERF3 observed range of rates for those magnitudes. This figure shows a 200-year span from the simulations. It is noteworthy that there are large variations in the moment and event rates for all the simulators. The moment and **M** 7+ event rates vary by a factor of 3 for all the simulators, and 200-year intervals can be found that differ significantly from other 200-year intervals. This forms the basis for the statements made in the Introduction that the simulators show variability on a time scale that our observations, certainly our instrumental observations, cannot show. However, it is true that the 95% confidence bounds of observational uncertainly represented in these figures (from fig. 15 of the UCERF2 report; Field *et al.*, 2008) allows such variability, as can also be seen in the frequency-magnitude plots of Figure 3. Again, event rates for ALLCAL and RSQSim fall within the observational

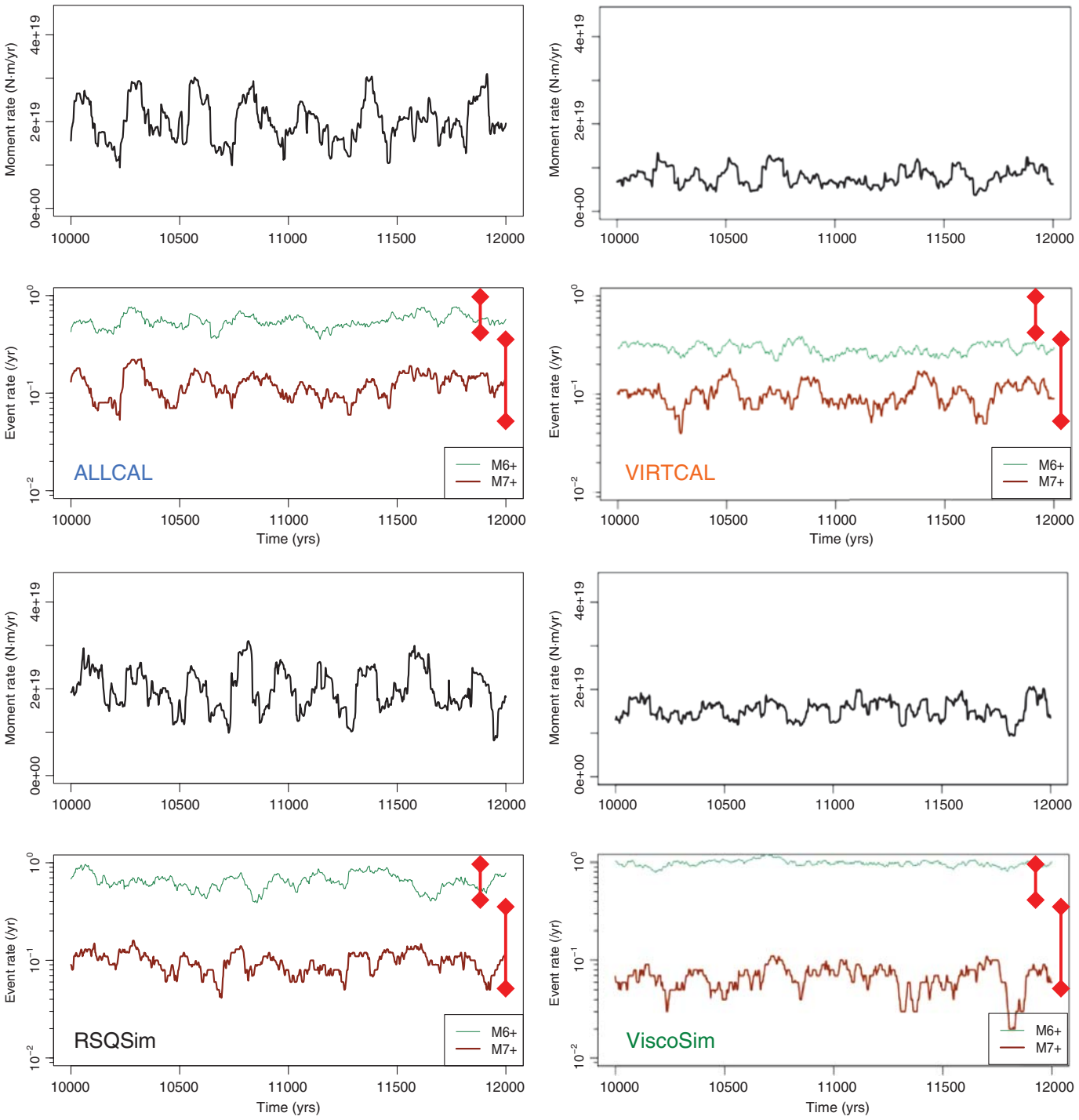

▲ **Figure 4.** Moment and event rates for a representative 2000-year time span from the 30,000-year simulations. Hundred-year moving averages are plotted. Red bars show the observed 95% confidence intervals for **M** 6+ and **M** 7+ rates (Field *et al.*, 2008). Note that simulated moment rates can differ by a factor of ~3 for periods of ~200 years, illustrating that the instrumental and historic records are too short to be representative samples of earthquake history.

bounds, whereas VIRTCAL is low for **M** 6+ events and ViscoSim is high for **M** 6+ events and low for **M** 7+ events.

The 100-year moving averages of moment rate for VIRTCAL are about a factor of 2 lower that those for ALLCAL and RSQSim for the 2000 years illustrated whereas the values for ViscoSim are intermediate. As it is not clear where the observed moment rates for California for the past 100 years fall within their likely range over a few thousand years, it is not clear how to compare observed-moment rate averaged over the past 100 years to the 100-year moving averages from the different simulators.

SCALING RELATION PLOTS

Plots of slip versus length, magnitude versus area, and magnitude versus length are shown in Figures 5–8. These include not only the data from our simulations, but also the data from three studies that include observations from events in California and around the world (Wells and Coppersmith, 1994; Hanks and Bakun, 2002; Ellsworth, 2003).

Figures 5 and 6 show the comparisons for slip-versus-fault length. Figure 5 shows results from all 30,000 years of simulations, whereas Figure 6 shows only 200 years of simulated events. We chose 200 years for Figure 6 because the observational data sets might be considered to contain roughly 200-years worth of California observations, as they consist of 100 years of California observations merged with numerous observations from other places around the world. In general, the mean of the results for most of the simulators is the same as the mean of the observations, but the number of outliers in the simulations is appreciably larger. This is particularly true when all 30,000 years of simulations are plotted and markedly less so when only 200 years of simulations are plotted, as one might

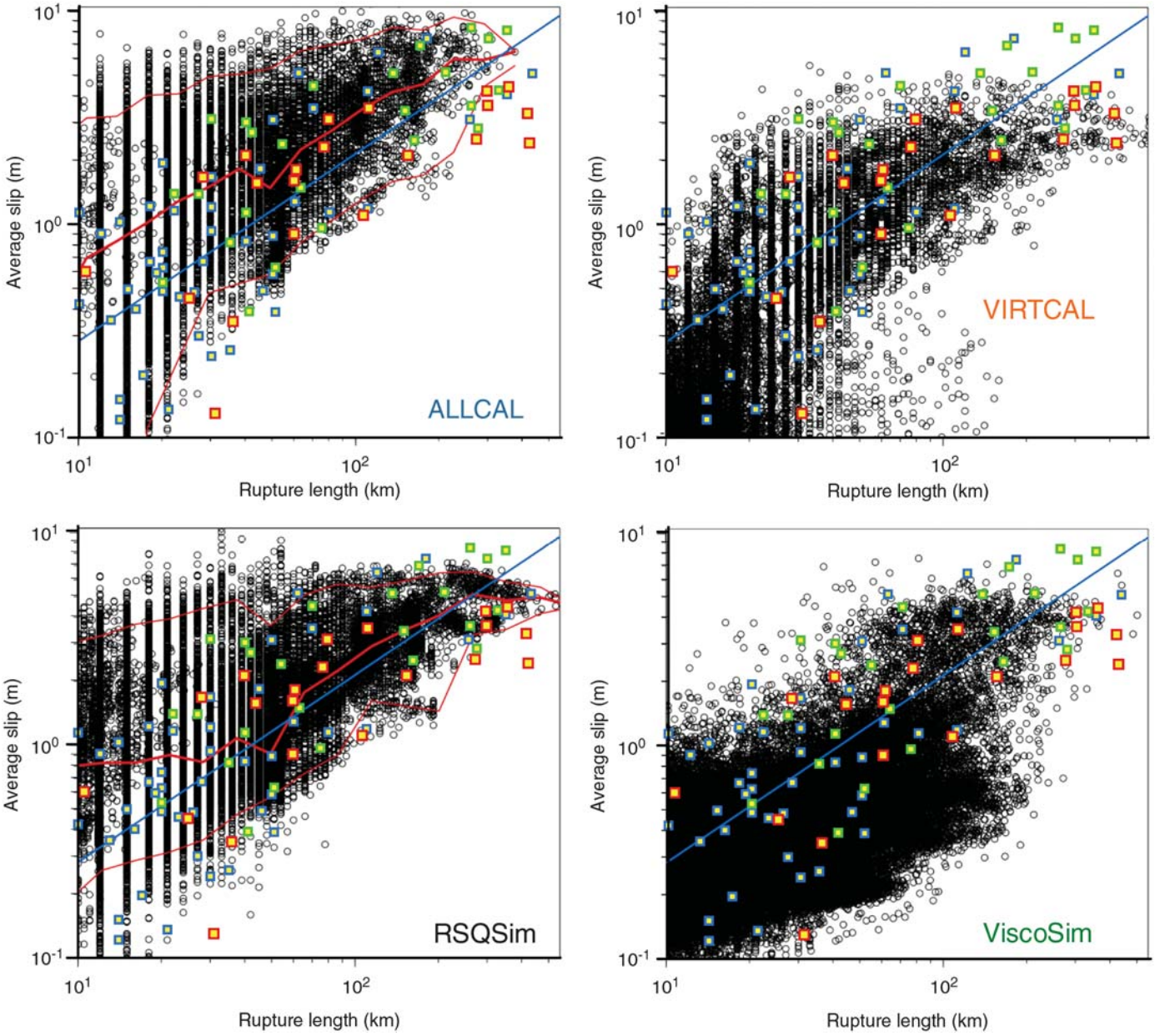

▲ **Figure 5.** Scaling of average slip versus rupture length. Our simulated values are shown in black; the observed scaling relations are shown in yellow with different-colored borders to indicate the source of the data: blue, Wells and Coppersmith (1994); green, Ellsworth (2003); and red, Hanks and Bakun (2002). The larger scatter for the simulation is in part due to its representing 30,000 years of history, whereas the worldwide data are for only ~100 years. Figure 6 shows simulations for only 200 years.

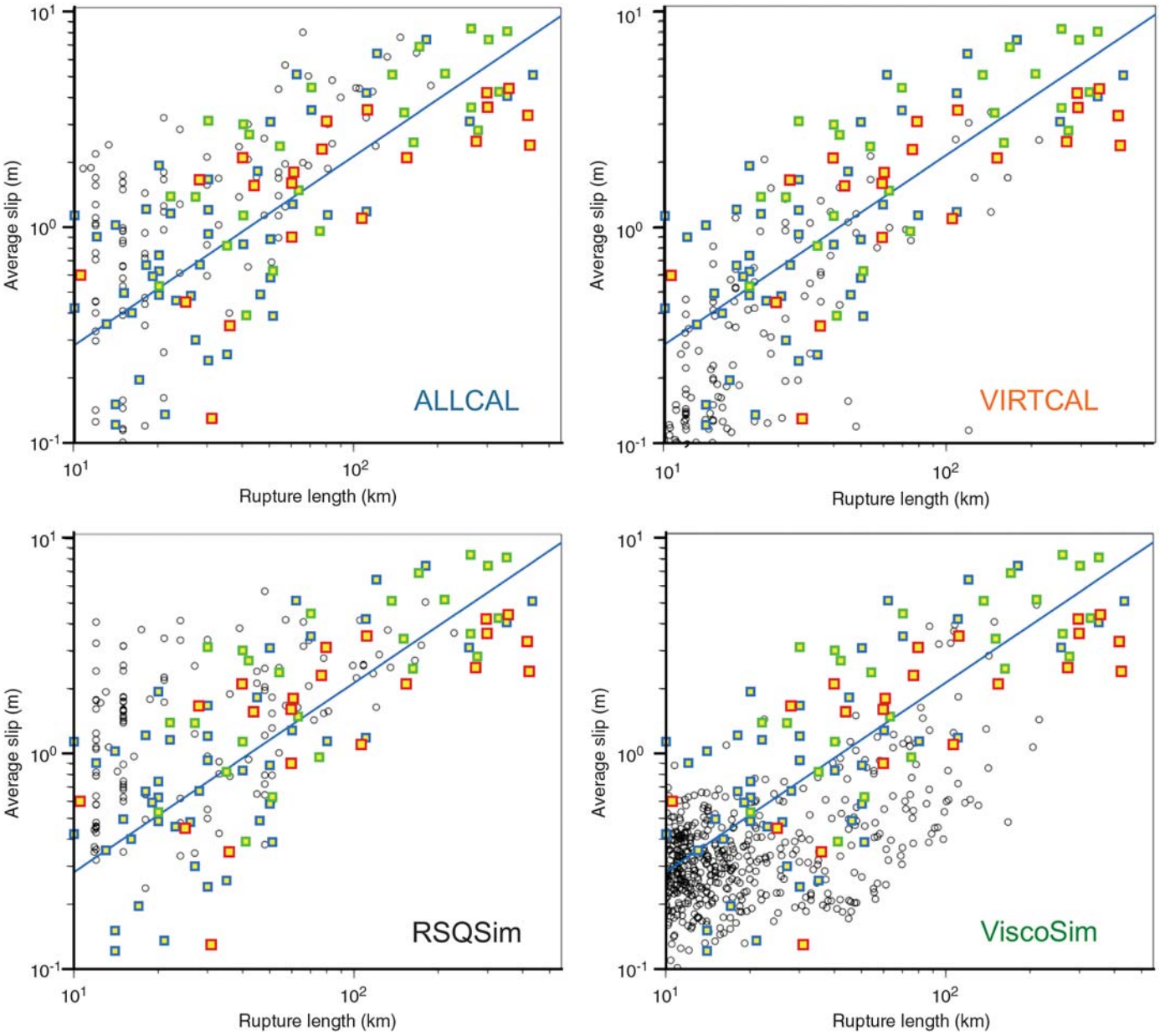

▲ **Figure 6.** Scaling of average slip versus rupture length for only 200 years of simulated history. Our simulated values are shown in black; the observed scaling relations are shown in yellow with different-colored borders to indicate the source of the data: blue, Wells and Coppersmith (1994); green, Ellsworth (2003); and red, Hanks and Bakun (2002). Here the 200 years of simulated events should be a time period that is more appropriate to compare with worldwide data for about 100 years, and the simulated scatter is similar to the observed.

expect. As for the frequency-magnitude plots, note that ALLCAL and RSQSim are similar to each other and closest to the observations, whereas ViscoSim is the farthest.

Magnitude-area scaling for all 30,000 years of simulation is shown in Figure 7. All the simulators match the observations, although RSQSim and ALLCAL fit the best, with RSQSim marginally better. The magnitudes for ViscoSim are lower than those of the other simulators or of the observations, and VIRTCAL is somewhat too high when compared with the observations. The same is true for only 200 years of simulations as shown in Ⓔ Figure S9 of the electronic supplement.

Finally, magnitude-length scaling is show in Figure 8 for all 30,000 years of simulation. Again, all fit the data reasonably, well with ALLCAL, VIRTCAL, and RSQSim fitting the best and the fit at the largest magnitude being marginally better for ALLCAL. Again, for this magnitude-length scaling, the magnitudes for ViscoSim are a bit too low. The same can be said for all the simulators when looking at only 200 years of

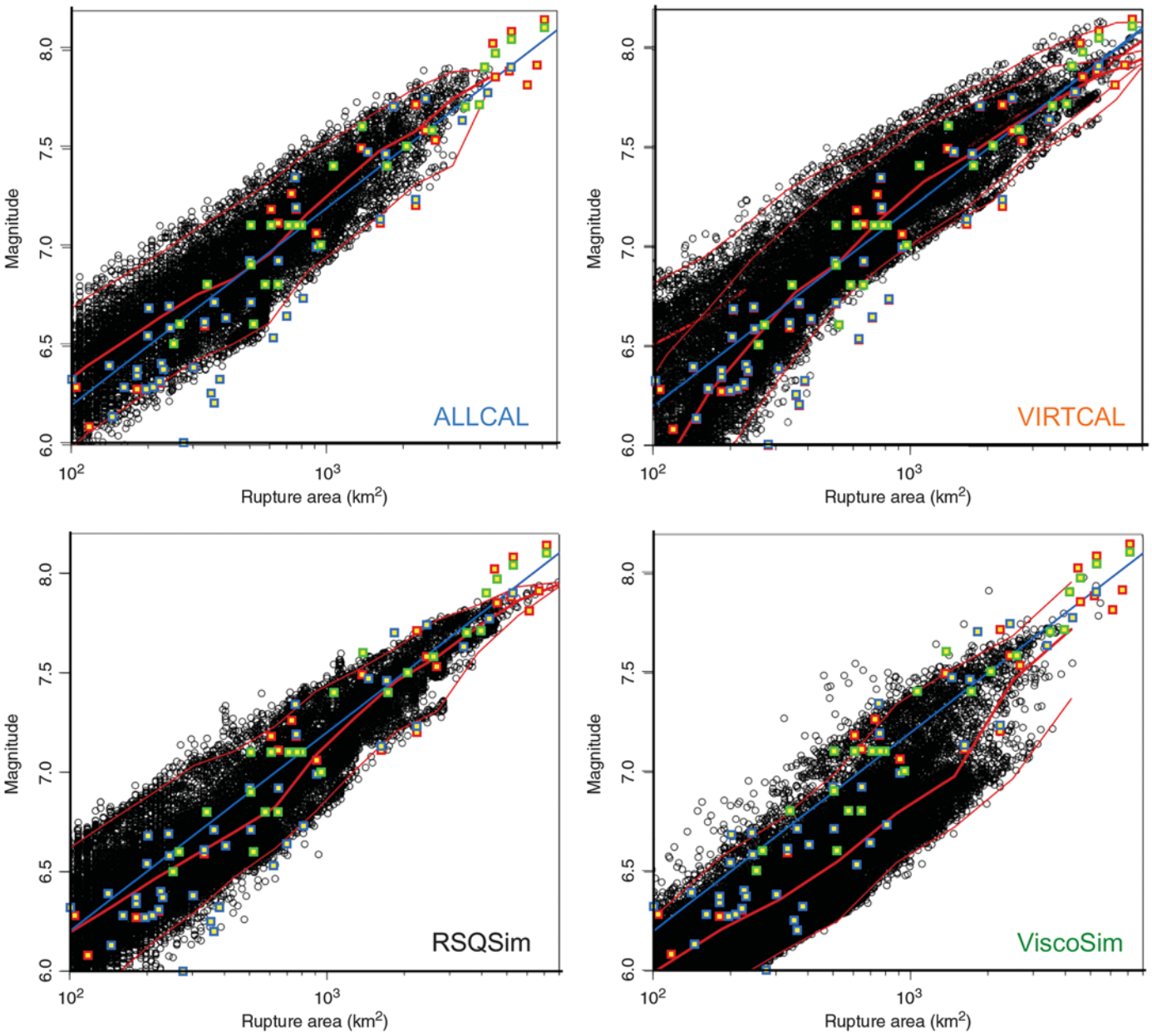

▲ **Figure 7.** Scaling of magnitude versus rupture area. Our simulated values are shown in black; the observed scaling relations are shown in yellow with different-colored borders to indicate the source of the data: blue, Wells and Coppersmith (1994); green, Ellsworth (2003); and red, Hanks and Bakun (2002). In a similar way to the difference between Figures 5 and 6 (comparing only 200 years of simulated seismicity, rather than 30,000 years), this figure shows scatter more similar to the observations as shown in Ⓔ Figure S9 of the electronic supplement.

simulated earthquakes, as shown in Ⓔ Figure S10 of the electronic supplement.

MEAN AND COVARIANCE OF INTEREVENT TIMES

We show in Figure 9 the values of the simulated interevent times and their covariance as a function of location in the fault system for two of the simulators, ALLCAL and RSQSim. Electronic versions of these plots as well as those for the other two simulators are available in Ⓔ Figures S11–S14 of the electronic supplement, where it is possible to enlarge the view to better examine the data and the labels on the fault segments.

Figure 9 also shows the observed preferred value and the maximum and minimum values for the observed interevent times from table 5 in appendix C of the UCERF2 report (Field *et al.*, 2008), including all 23 locations for which this data is available from paleoseismic observations. As described in Tullis *et al.* (2012), these paleoseismic data are the constraint used by the simulators to tune the strength drops for those fault sections containing the locations of the 23 available paleoseismic sites. This data is also shown in Figure 10. To produce the simulated interevent times shown in these figures, the fault-strength drops have been adjusted by trial and error so that

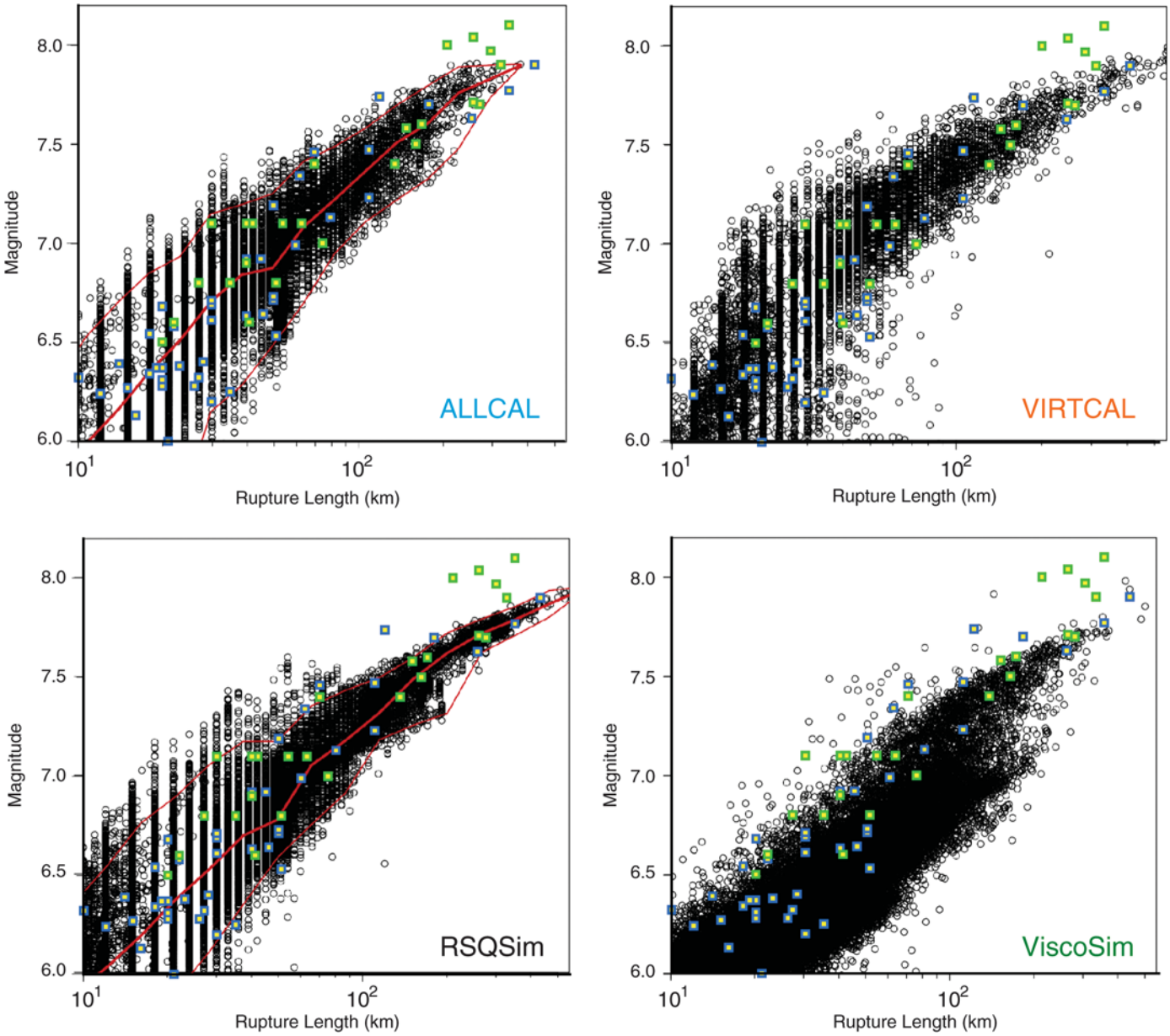

▲ **Figure 8.** Scaling of magnitude versus rupture length. Our simulated values are shown in black; the observed scaling relations are shown in yellow with different-colored borders to indicate the source of the data: blue, Wells and Coppersmith (1994), and green, Ellsworth (2003). In a similar way to the difference between Figures 5 and 6 (comparing only 200 years of simulated seismicity, rather than 30, years), this figure shows scatter more similar to the observations shown in Ⓔ Figure S10 of the electronic supplement.

the simulated recurrence intervals match the mean of the observed values for each of the 23 sites. However, Figures 9 and 10 show the trial-and-error process was not maintained in order to make a perfect match, as was done in the case of the Caleveras and Garlock faults, for example.

The coefficient of variation of the recurrence times for all the major faults lies mostly in the range of about 0.3–0.7, with a few that are larger. More detail on the variability in recurrence time can be seen from the probability distribution functions of Figure 10 and Ⓔ Figures S15–S30 of the electronic supplement.

PROBABILITY DISTRIBUTION FUNCTIONS OF RECURRENCE INTERVALS

The added information shown in Figure 10 (beyond that in Fig. 9) is the probability distribution functions (PDFs) of the recurrence intervals. Although we have such plots for many sites and all simulators, the data shown in Figure 10 are representative of the variability. Many additional examples are shown in Ⓔ Figures S15–S30 of the electronic supplement, including plots for all the simulators and the 23 sites having paleoseismic data. The comparisons between the simulators and the data and between different simulators show a range

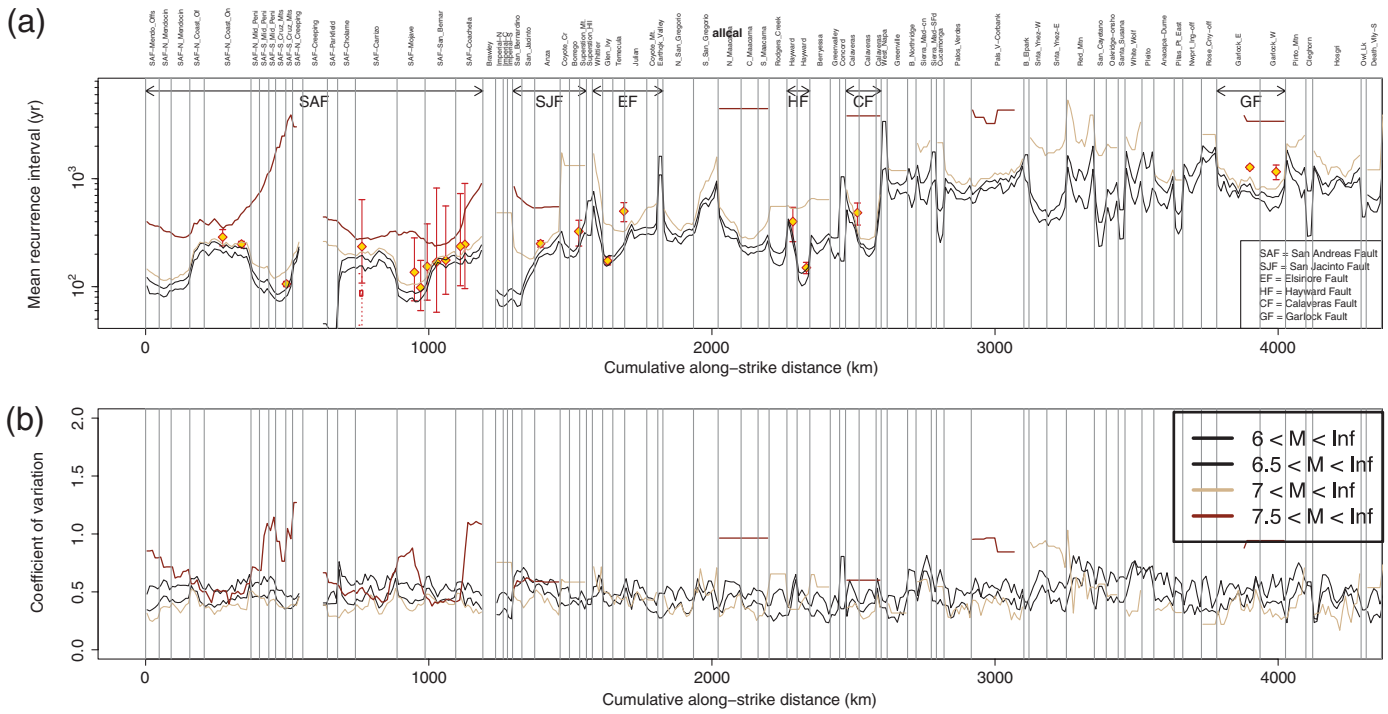

▲ **Figure 9.** (a) Mean and (b) covariance of interevent times arranged by section for the major faults. This example is for the ALLCAL simulator and at the printed scale is hard to read, but this and similar diagrams of the other three simulators are in Ⓔ Figures S11–S14 of the electronic supplement on a scale that allows the fault section names to be more clearly viewed. The line colors correspond to the magnitude range as shown in the key. For sites having paleoseismic data on recurrence intervals, the preferred value (RI) from the UCER2 report, appendix C, table 5 (Field *et al.*, 2008) is shown as a diamond, and the bars show their table 5 RI "Max" and "Min." Examples of the probability-distribution functions for recurrence intervals are shown in Figure 10 and Ⓔ Figures S15–S30 of the electronic supplement show functions for all 23 sites having paleoseismic data for all four simulators.

of behavior represented in Figure 10. Some sites have a smaller observational range between the maximum and minimum values than the range shown by the 90% confidence intervals (e.g., San Andreas, North Coast), and some have the situation reversed (e.g., San Andreas, Carrizo Plain). It is important to note that the quantitative comparison between our 95% confidence intervals and the maximum and minimum range given in the UCERF2 report is not appropriate because they correspond to different measures of the variability. One problem in comparing the recurrence intervals from the simulations with those observed via paleoseismology is that it is not clear what magnitude of earthquakes may be recorded in the paleoseismic record. For example, the illustrated PDF of simulated recurrence intervals for the South Hayward fault is quite different for **M** 6.5+ and for **M** 7+ events, but we do not know for which earthquake magnitude the results should be tuned to fit the observed recurrence interval.

TIME-INDEPENDENT FORECASTS

The simulators also produce time-independent forecasts of the expected number of events per year as a function of magnitude and location. An example of this for the ALLCAL simulator is shown in Figure 11. Similar plots for the other simulators are given in Ⓔ Figures S31–S34 in the electronic supplement, and they are quite similar to what is illustrated in Figure 11. Although such forecasts have not yet been attempted, they are suitable for testing against observations via the methodology of the Collaboratory for the Study of Earthquake Predictability (http://www.cseptesting.org/). However, a long period of time would have to pass before such tests would be conclusive for the **M** 6 earthquakes shown in Figure 11 because of the infrequency of earthquakes of this size. Once simulator results are obtained for smaller and hence more frequent earthquakes, such tests could be completed more quickly. Simulating smaller earthquakes would require using finer grids than the present ~3-km squares and satisfactorily dealing with the occurrence of earthquakes on nonmodeled faults and off-fault seismicity.

TIME-DEPENDENT CONDITIONAL PROBABILITIES

Although much more exploration of the time-varying probability of earthquake occurrence in time and space could be done with the earthquake catalogs generated by the simulators, Figure 12 shows an intriguing example of such data. The question often arises when an earthquake occurs as to how the probability of occurrence of a nearby earthquake will change? Figure 12a shows that for effects on faults that are remote from an earthquake (for example, effects on the Calaveras fault following an **M** 6.5+ event on the San Jacinto fault), the conditional probability is the same as at any other time. Thus, as expected, the San Jacinto fault does not affect the Calaveras

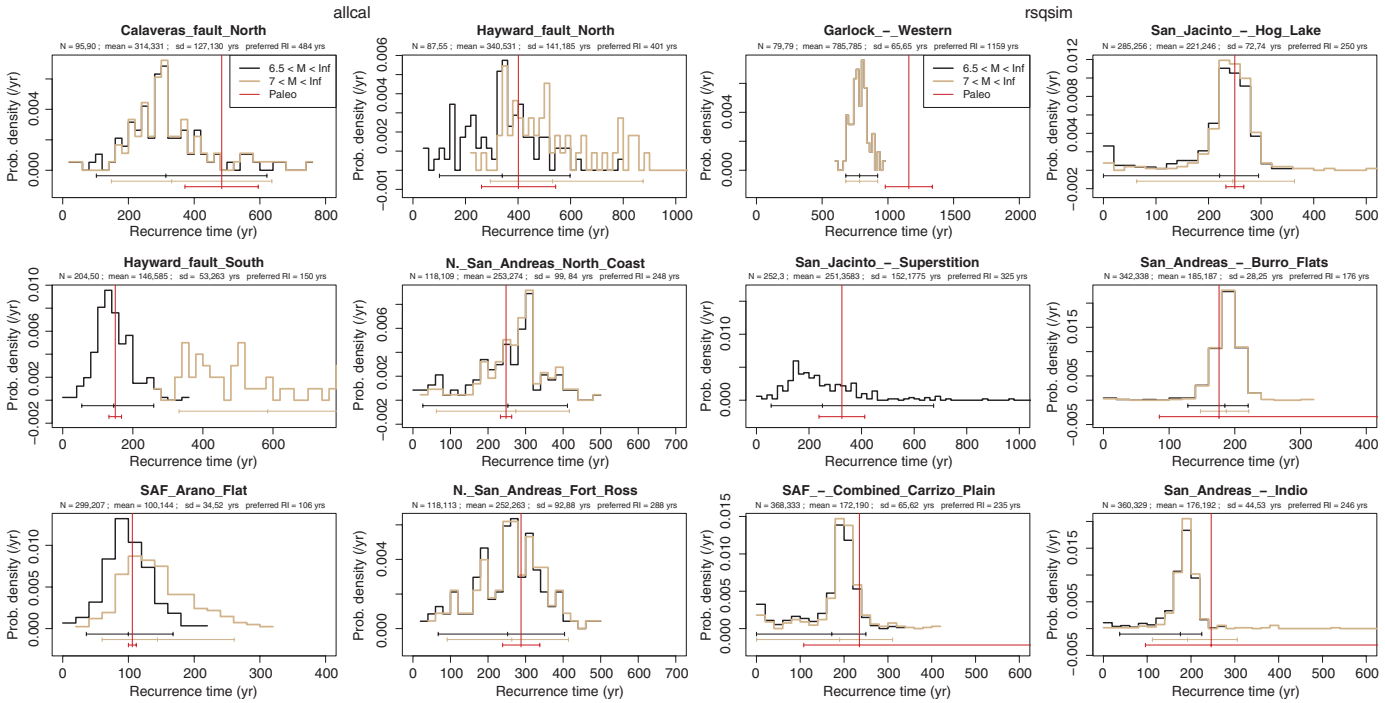

▲ **Figure 10.** Probability distribution functions of recurrence intervals for **M** 6.5+ (black) and **M** 7+ (brown) events at 12 paleoseismic sites and for two earthquake simulators. Also shown in red are inferred mean, minimum, and maximum recurrence values at these sites (Field *et al.*, 2008). These only give some estimate of the observed range and are not comparable with the 95% confidence intervals shown for the simulations. The strength-drop values used have been adjusted so the simulated recurrence intervals approximately match the observed means for those fault sections with paleoseismic sites. However, questions exist about the size of events that would be identified at such sites. Similar plots for all simulators and all 23 paleoseismic sites are shown in Ⓔ Figures S15–S30 of the electronic supplement.

fault. However, this is not true for nearby faults. As demonstrated in Figure 12b, all the simulators show that there is a decrease in the conditional probability of a subsequent **M** 6.5+ on the nearby fault relative to random times (black curves lies above red curves), extending from about 10 to 200 years after the initial **M** 6.5+ event. This is a manifestation of the fact that many times both the San Jacinto and Anza sections of the San Jacinto fault break in the same event; and, due to the reloading required by elastic rebound, which is integral to all the simulators, there is about a 200-year quasi-periodicity in the occurrence of events on these sections (as seen in Fig. 9 and Ⓔ Figs. S11–S14 of the electronic supplement). As shown in Figure 12b for the RSQSim simulator, if an **M** 6.5+ event occurs on the Anza section of the San Jacinto fault, the conditional probability of an **M** 6.5+ earthquake occurring on the adjacent San Jacinto section of the San Jacinto fault is appreciably increased for the next 10 years (black curve lies above red curve). This effect is only present in the RSQSim simulator because it alone uses rate and state friction, which includes nonlinear changes in slip rate as a function of stress.

AFTERSHOCKS

RSQSim is the only one of our simulators that exhibits aftershocks, as shown in Figure 12c. The figure shows that there is a greatly increased probability of occurrence of **M** 5+ earthquakes following the occurrence of an **M** 7+ earthquake. This figure does not show the additional fact that the spatial distribution of the subsequent smaller earthquakes shows them to be near the mainshock as is the case for real aftershocks.

DISCUSSION

The rationale behind earthquake simulators is that we know enough about the physics of earthquakes that it is possible to create a series of synthetic earthquakes that bear a reasonable resemblance to reality. Different aspects of the physics are understood to various extents. The most fundamental aspect of the physics is that the slip on a fault at one location causes changes in stress elsewhere in the system, and this can be approximated by dislocations in a linear-elastic half-space. All our simulators include such behavior. One, ViscoSim, includes viscous relaxation of deeper levels of the lithosphere as well as layered elasticity. Our tests to date do not show that this additional complexity has a significant effect on the earthquake history. If such effects exist, they are masked by other differences between the simulators.

True elastodynamic stress transfer and stress concentrations are not possible in these quasi-static or quasi-dynamic simulations (see Lapusta *et al.*, 2000, for a definition), thus the dynamic stress concentrations at the tip of propagating

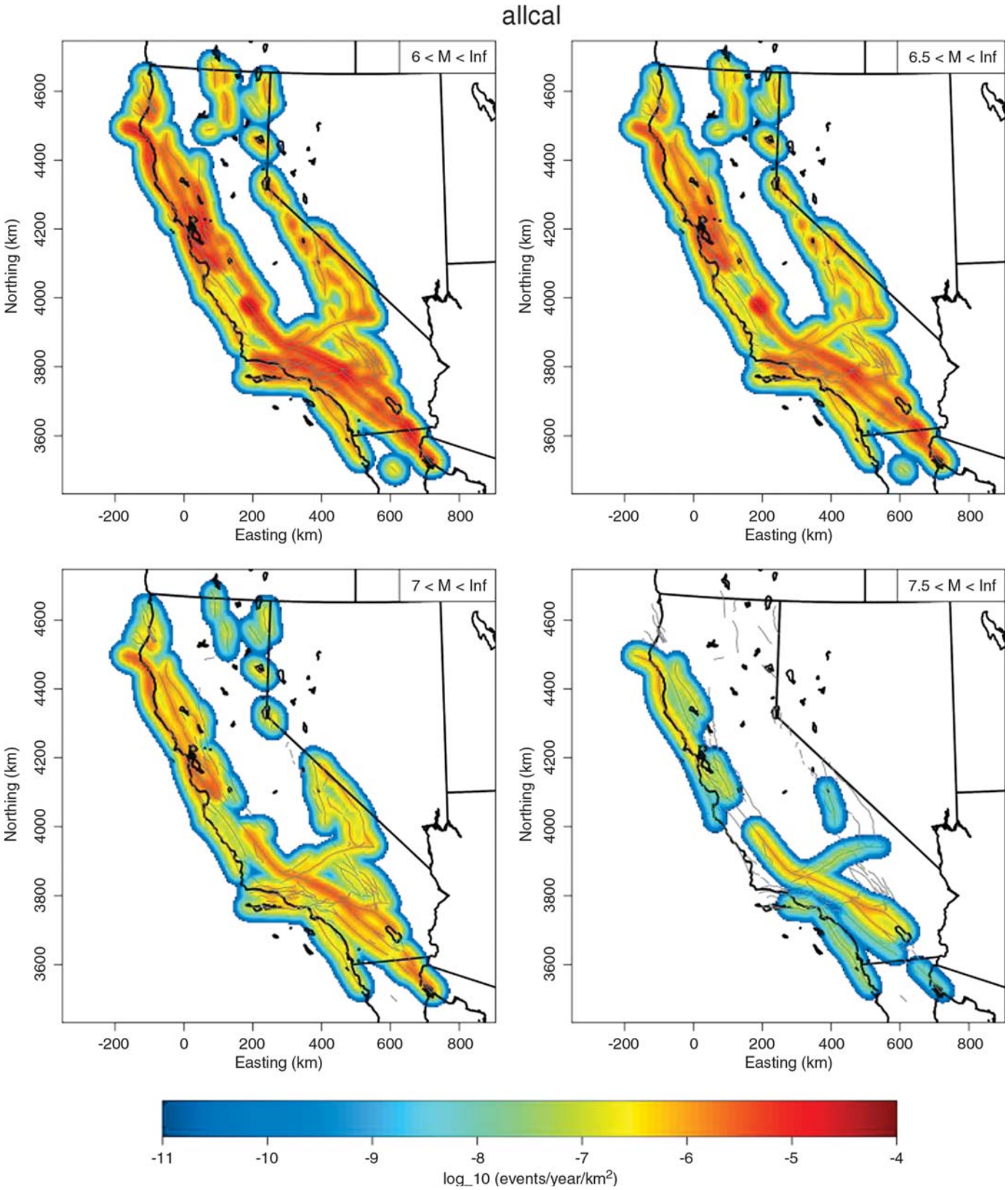

▲ **Figure 11.** Earthquake density in events per year per km^2 for magnitudes greater than 6, 6.5, 7, and 7.5 from one simulator. Results for other simulators are similar but differ somewhat. All are shown as Ⓔ Figures S31–S34 of the electronic supplement.

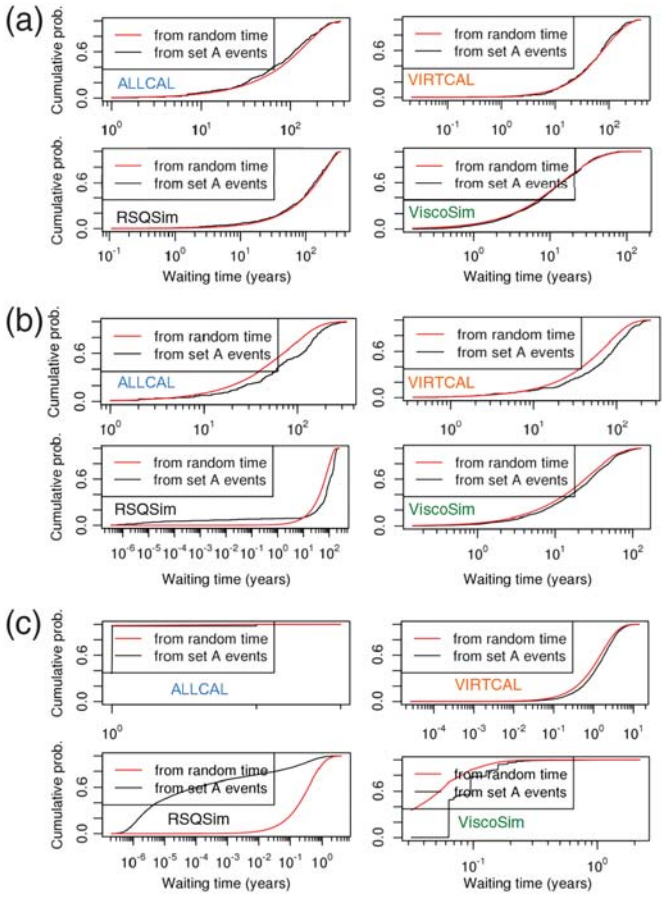

▲ **Figure 12.** Conditional probabilities of one type of event following the occurrence of another type of event versus time. The red curves in all plots represent the null hypothesis and involve random times for the occurrence of the initial event, and the black curves represent the actual relative timing of the initial and subsequent events. Both parts (a) and (b) are the conditional probabilities of an **M** 6.5+ event occurring on some fault section, as a function of time after an **M** 6.5+ event on another fault section. In both parts (a) and (b), the first event is on the Anza section of the San Jacinto fault. In (a) the subsequent event is on the Calaveras where no causality is expected, whereas in (b) it is on the San Jacinto section of the San Jacinto, where some earthquake clustering might occur. Part (c) shows the probability of occurrence of an **M** 5+ event occurring following the occurrence of an **M** 7+ event, namely the occurrence of aftershocks.

earthquake ruptures does not occur. However, by weakening adjacent elements following the slip of a given element, a similar difference between applied stress and strength can be achieved, and we find this approximate treatment causes a significant effect. This is shown by the contrast in behavior between VIRTCAL, which has enhanced rupture weakening and produces fewer small earthquakes, and ViscoSim, which has no rupture-weakening parameter and produces fewer large earthquakes and more frequent small ones (Fig. 2).

Another important consideration is the constitutive property of the fault zone. The RSQSim simulator with the most complex constitutive behavior, an approximation to rate and state friction, seems to fit all the observational data slightly better than any of the other simulators. It is the only simulator that shows the occurrence of time-dependent increases in conditional probability of nearby earthquakes following a significant earthquake (Fig. 12b) as well as aftershocks (Fig. 12c). Perhaps related to the fault constitutive complexity, the simulator that fits the observational data nearly as well as RSQSim is ALLCAL, which is the only simulator besides RSQSim that has velocity dependence in its friction.

Thus our comparisons between the simulators and data and among the simulators show that several features of the simulators may be important in making them fit observations, with rupture weakening and fault friction treatment being important. Given the large numbers of faults cutting different geological materials, the details of the spatial variation of fault-constitutive properties, simplified as strength drops, cannot be properly defined by the limited knowledge we have of the fault properties. Variations in strength drops result in variations in recurrence interval, and we have constraints from valuable data on this occurrence at 23 paleoseismic sites. Although improved data at more such sites would be very valuable, it is unlikely that we will ever know as much about the fault-constitutive properties as would be desirable. Nevertheless, by fitting the parameters in the simulators to the limited observational data from the instrumental, historical, and paleoseismological record, we show that simulators can reproduce the observations. The promise of the simulators is that once they are fit to all the available data, they may have predictive value that extends beyond these data.

It should be noted that these simulators presently only represent seismicity on the explicitly modeled faults, whereas actual seismicity occurs elsewhere, both on nonmodeled faults and as off-fault background seismicity. In the future, it is likely that such seismicity can be included in a variety of ways, but this has not been done to date with the simulator results we present here. Furthermore, smaller events are less likely to be included in our simulations because they occur on smaller faults, which are either not yet included or not yet recognized. Reducing the element size used to represent the faults below the ~3 km we used in this study will allow better representation of smaller events. However, only if many smaller faults are included, either explicitly or via some approximate treatment, can reducing the element size hope to deal adequately with small events.

In spite of the limitations of the instrumental, historical, and paleoseismological records, these observational data appear to adequately define a significant quantity of the unknown data that one would ideally have concerning the fault system. Even though the simulators fit this available data, they show variations in earthquake rates over longer periods of time than are represented by the data. Thus, the physics of the system, including the interactions between the earthquakes that occur, produce behavior that goes beyond what we have been able to observe. This is encouraging for the value of physics-based earthquake simulators in increasing our understanding of

earthquake physics and learning more about hazard and its time dependence.

SUMMARY

The simulators show general agreement with one another and with limited observational data of various types, although the differences are not perfect in some cases. The frequency-magnitude distributions are close to those observed but not exactly the same; given that not all the seismicity in the observed frequency-magnitude distribution falls on the faults in our allcal2, how well the simulated distributions should fit the data is debatable. In general, ALLCAL and RSQSim seem in somewhat better agreement with all the various data, whereas ViscoSim agrees the least. Many statistical measures of simulator behavior can be extracted from the long synthetic earthquake catalogs that cannot be drawn from the much shorter observational record. This fact, coupled with the simulators' apparent realism, offers encouragement for future simulator development and use in understanding earthquake physics and hazard.

ACKNOWLEDGMENTS

This research was supported by the Southern California Earthquake Center. SCEC is funded by National Science Foundation Cooperative Agreement EAR-0529922 and U.S. Geological Survey Cooperative Agreement 07HQAG0008. The SCEC contribution number for this paper is 1599.

REFERENCES

Barall, M. (2012). Data transfer file formats for earthquake simulators, *Seismol. Res. Lett.* **83,** no. 6, 991–993.

Ellsworth, W. L. (2003). Magnitude and Area Data for Strike Slip Earthquakes, Appendix D, Earthquake Probabilities in the San Francisco Bay Region: 2002–2031, *U.S. Geol. Surv. Open-File Rept. 2003-214*.

Field, E. H., T. E. Dawson, K. R. Felzer, A. D. Frankel, V. Gupta, T. H. Jordan, T. Parsons, M. D. Petersen, R. S. Stein, R. J. Weldon II, and C. J. Wills (2008). The Uniform California Earthquake Rupture Forecast, Version 2 (UCERF 2), *U.S. Geol. Surv. Open-File Rept. 2007-1437*.

Hanks, T. C., and W. H. Bakun (2002). A bilinear source-scaling model for M – log A observations of continental earthquakes, *Bull. Seismol. Soc. Am.* **92,** no. 5, 1,841–1,846, doi: 10.1785/0120010148.

Lapusta, N., J. Rice, Y. Ben-Zion, and G. Zheng (2000). Elastodynamic analysis for slow tectonic loading with spontaneous rupture episodes on faults with rate- and state-dependent friction, *J. Geophys. Res.* **105,** 23,765–23,789.

Pollitz, F. F. (2012). ViscoSim earthquake simulator, *Seismol. Res. Lett.* **83,** no. 6, 979–982.

Richards-Dinger, K., and J. H. Dieterich (2012). RSQSim earthquake simulator, *Seismol. Res. Lett.* **83,** no. 6, 983–990.

Sachs, M. K., M. B. Yikilmaz, E. M. Heien, J. B. Rundle, D. L. Turcotte, and L. H. Kellogg (2012). Virtual California earthquake simulator, *Seismol. Res. Lett.* **83,** no. 6, 973–978.

Tullis, T. E., K. Richards-Dinger, M. Barall, J. H. Dieterich, E. H. Field, E. M. Heien, L. H. Kellogg, F. F. Pollitz, J. B. Rundle, M. K. Sachs, D. L. Turcotte, S. N. Ward, and M. B. Yikilmaz (2012). Generic earthquake simulator, *Seismol. Res. Lett.* **83,** no. 6, 959–963.

Ward, S. N. (2012). ALLCAL earthquake simulator, *Seismol. Res. Lett.* **83,** no. 6, 964–972.

Wells, D. L., and K. J. Coppersmith (1994). New empirical relationships among magnitude, rupture length, rupture width, rupture area and surface displacement, *Bull. Seismol. Soc. Am.* **84,** no. 4, 974–1,002.

Terry E. Tullis
Brown University
Department of Geological Sciences
Providence, Rhode Island 02912-1846 U.S.A.
terry_tullis@brown.edu

Keith Richards-Dinger
James H. Dieterich
University of California, Riverside
Department of Earth Sciences
Riverside, California 92521 U.S.A.

Michael Barall
Invisible Software, Inc.
P.O. Box 6541
San Jose, California 95150 U.S.A.

Edward H. Field
U.S. Geological Survey
1711 Illinois Street
Golden, Colorado 80401 U.S.A.

Eric M. Heien
Louise H. Kellogg
Donald L. Turcotte
M. Burak Yikilmaz
University of California, Davis
Department of Geology
Davis, California 95616-8605 U.S.A.

Fred F. Pollitz
U.S. Geological Survey
345 Middlefield Road, MS 977
Menlo Park, California 94025 U.S.A.
fpollitz@usgs.gov

John B. Rundle[1]
Michael K. Sachs
University of California, Davis
Department of Physics
Davis, California 95616 U.S.A.

Steven N. Ward
University of California, Santa Cruz
Institute of Geophysics and Planetary Physics
Santa Cruz, California 95064 U.S.A.

[1] Also at Department of Geology, University of California, Davis, California 95616 U.S.A.; and Santa Fe Institute, 1399 Hyde Park Road, Santa Fe, New Mexico 87501 U.S.A.